ROYAL SOCIETY
OF CHEMISTRY

FEATURE ARTICLE

Check for updates

Continuum *vs.* atomistic approaches to computational spectroscopy of solvated systems

Tommaso Giovannini [iD] and Chiara Cappelli [iD] *

Molecular spectral signals can be significantly altered by solvent effects. Among the many theoretical approaches to this problem, continuum and atomistic solvation models have emerged as the most effective for properly describing solvent effects on the spectroscopic signal. In this feature article, we review the continuum and atomistic descriptions as applied to the calculation of molecular spectra, by detailing the similarities and differences between the two approaches from the formal point of view and by analyzing their advantages and disadvantages from the computational point of view. Various spectral signals, of increasing complexity, are considered and illustrative examples, selected to exacerbate the differences between the two approaches, are discussed.

1. Introduction

The role of computational chemistry to assist experimental studies has grown substantially in the last decades. This is due to the increasing availability of user-friendly computational packages, which can be used also by non-specialists. Furthermore, the success of computational approaches follows the development of methods that can treat with considerable accuracy large, complex, and realistic chemical systems.[1–5]

In parallel, computational spectroscopy, *i.e.* the calculation of spectral properties by means of computational methods, has become an invaluable tool in most fields of chemical research.[6] In fact, thanks to the high level of accuracy that has been reached in the reproduction of experimental data in the condensed phase, it often provides a theoretical rationalization of many experimental findings, yielding truly synergistic investigations.[7–9] In fact, although many algorithms of increasing accuracy have been proposed and tested for systems in the gas phase,[10–12] the large majority of molecular spectra are routinely measured in the condensed phase, *i.e.* when chemical systems are dissolved in a solvent or other kinds of external environments (biological matrix, polymeric materials, crystal phase *etc.*). Indeed, molecular structure and response to external electromagnetic fields can be significantly altered by the environment, thus making the simulation for isolated systems mostly inappropriate for a reliable comparison with experimental findings.[13–16]

Effective theoretical modeling of spectroscopy in the condensed phase requires catching the physico-chemical features of the simultaneous interaction of a chemical system with the

Scuola Normale Superiore, Piazza dei Cavalieri 7, 56126 Pisa, Italy.
E-mail: chiara.cappelli@sns.it

environment and the external radiation field.[1,17–20] Since spectroscopy arises from the interaction between the molecule and the radiation, which is in general driven by the electronic component, reliable modeling needs to resort to Quantum-Mechanical (QM) descriptions. However, while such approaches may be feasible for small-to-medium molecules in the gas phase, for systems in the condensed phase a "brute-force" description, *i.e.* which treats all atoms at the QM level, is unfeasible due to the enormous number of degrees of freedom that would need to be taken into account. However, such a description would be useless in most cases; in fact, the electronic structure of the environment would be described, however it commonly does not drive the spectral signal of chemical systems in the condensed phase.[21,22] In fact, it is universally recognized that molecular spectra are modified but not determined by the environment, and this is indeed an important concept, which lays the foundations for the spectroscopic identification of molecular structures.

Focused models[1,13,19,23–25] are the most successful class of approaches to computational spectroscopy in the condensed phase. There, the focus is the target molecule (solute in case of solutions) and the key is the accurate modeling of molecule/environment interactions and their consequences on the molecular structure and properties.[17,18,20,26] The intrinsic spectral properties of the environment are not modelled, which corresponds to assuming molecular properties to be local properties of the molecule, which can be modified but not determined by the presence of the environment.

The most renowned class of focused models belongs to the family of multiscale (multilayer) QM/classical approaches.[23] The latter have had great success in modern chemical research because they can be effectively coupled with most QM descriptions, ranging from semi-empirical methods[27,28] to Density

Functional Theory (DFT) or Wavefunction Theory.[29–32] Remarkably, there is no substantial increase in computational cost with respect to the corresponding QM calculation of the isolated molecule because the number of degrees of freedom to be treated at the QM level does not change. Also, the machinery of Quantum Chemistry can be exploited to obtain the desired spectral signals in the same way as they are calculated for isolated systems.[17–19] In fact, additional environment-related terms are introduced in the molecular Hamiltonian, which results in extra terms appearing in the formulation of energy derivatives and response equations.[19]

The main difference among the various types of focused QM/classical models stays in the way the environment is modelled. Implicit (continuum) or explicit (atomistic) approaches have been proposed: the former is especially suited to treat solvents,[13] whereas fully atomistic descriptions may treat all kinds of environments, pending suitable parametrizations.[1,2,27,33,34] In continuum solvation approaches, the atomistic nature of the solvent is neglected and the solvent is modelled in terms of a continuum dielectric, featuring specific dielectric properties. The Polarizable Continuum Model (PCM),[13] has been particularly successful in the context of the present paper, because it has been extended to a large variety of spectral signals and molecular properties.[17,18] A clear bottleneck of the QM/PCM approach, and in general of all implicit approaches, is their severe limitation in describing specific and directional solute–solvent interactions, such as hydrogen bonding. To this end, explicit approaches have been developed, belonging to the family of QM/Molecular Mechanics (QM/MM) methods.[1,19,23,35,36] There, the target molecule is still described at the QM level, but the environment (solvent) is treated by resorting to MM force fields. QM/MM fully atomistic descriptions are not gained for free: in fact, whereas continuum models include implicitly the statistical average of all possible solute–solvent configurations, QM/MM approaches require the explicit sampling of the solute–solvent phase space.[1,37] However, they provide a dynamic description of the solvation phenomenon, which basic continuum formulations lack.

In this feature article, we discuss continuum and atomistic solvent descriptions as applied to the calculation of the molecular spectra. First, we detail similarities and differences between the two approaches from the formal point of view, followed by a discussion of the advantages and disadvantages of the two methods, also from the computational point of view. Then, we discuss how to specify the models to catch the physics of the solvated system and transfer it to the computation of various spectral signals, of increasing complexity. Finally, some specific examples are discussed, especially suited to illustrate the concepts highlighted in the theoretical discussion. Some conclusions end the manuscript.

2. Continuum vs. atomistic modeling of solvation

Historically, focused models derive from the approach first presented by Onsager in 1936.[38] In this rather crude model,

the solute is represented as a permanent point dipole with a given polarizability, and is placed at the center of a spherical cavity surrounded by the solvent, which is viewed as a continuum dielectric medium. In the absence of external fields, an electric field is originated, which directly depends on the polarization of the solvent as a response to the solute's permanent dipole. At the same time, the solvent back-polarizes the solute. This electric field is named "reaction field", and it is a fundamental concept underneath all polarizable approaches, either explicit or implicit.[13,39,40]

In modern implicit approaches, the solvent is still described in terms of a homogeneous polarizable continuum, featuring an electric permittivity constant ε.[13,41,42] However, the simplistic approach proposed by Onsager is ameliorated in two directions. First, the solute is not approximated by a point-like dipole but is treated in terms of a quantum mechanical wavefunction/density. Second, the solute is accommodated in a molecular-shaped cavity, which is generally constructed in terms of interlocking spheres centered on each solute atom.[43,44] The presence of the solute density polarizes the dielectric, yielding the formation of an apparent charge density on the cavity surface, which back-polarizes the solute, consistently with the concept of reaction field introduced by Onsager.[13] The surface charge density is named apparent because it only exists in the presence of the solute; in the computational practice, it is discretized in a set of apparent surface charges (ASC), which are the solution of the Poisson equation with appropriate boundary conditions.[45,46]

The interaction between the solute and solvent is generally limited to electrostatics and mutual polarization terms; their inclusion into the QM/PCM Hamiltonian results in the remarkable feature that solvent-depend terms propagate to the calculation of molecular properties and spectroscopies through response equations/derivatives.[17,18,47] Note that the limitation to electrostatic terms is a reasonably good approximation for polar solvents with large ε, however non-electrostatic (Pauli repulsion and dispersion) should also be considered, for instance by means of one of the methods which have been developed for this purpose.[25,48–53]

Clearly, in implicit models solvent molecules are not actually considered; thus, solute–solvent interactions, e.g. Hydrogen Bonding, are neglected. However, one of the most attractive aspects of continuum models is that their description can systematically be improved, for instance by including some (few) solvent molecules, in the so-called "cluster" or supermolecule models.[54] Solvent molecules can be treated at the same QM level of the solute, or a lower level, for instance by resorting to ONIOM schemes.[55] Clearly, in this way first-shell specific solute–solvent interactions can be described, however, it is not straightforward to define the number of solvent molecules to include, and especially their positions, i.e. how many configurations need to be considered to get reliable modeling.

A way to solve this problem, with additional advantages that will be discussed in the following presentation, consists of fully recovering the solvent atomistic nature and moving to explicit

modeling, *i.e.* to QM/MM.[35] There, the solute is described at the QM level, whereas the environment is described by resorting to MM force fields, therefore the problem shifts to the description of the interaction between the QM and MM portions. In this respect, different approximations have been proposed:[35]

• Mechanical embedding: the QM/MM coupling term is treated at the MM level only, therefore it is independent of the QM electronic density. The coupling is expressed in terms of dispersion–repulsion potentials (usually, the Lennard-Jones potential) and classical electrostatics. Thus, the contribution of the surrounding environment to the energy and properties of the QM portion is only indirect.

• Electrostatic embedding: MM atoms are endowed with fixed atomic charges, that produce an electric potential, which polarizes the QM electronic density. From the point of view of the QM solute, electrostatic embedding introduces a new term in the molecular Hamiltonian, that is the interaction between the potential generated by the MM fixed charges and the electron density. Dispersion – repulsion contributions are usually considered by resorting to classical potentials.

• Polarizable embedding: the mutual polarization between MM and QM portions is explicitly taken into account, thus recovering the concept of reaction field. Polarizable embedding work in such a way that the MM force field contains a response term, which modifies electrostatics due to the presence of the QM density. A polarization term is included in the QM Hamiltonian to represent the interaction between the electronic density and the MM portion. Also in this case, dispersion-repulsion contributions are treated in terms of classical potentials.

Among the several QM/Polarizable Embedding schemes that have been proposed in the literature,[19,39,56–64] the most similar to the continuum approach, from the formal point of view, is the QM/Fluctuating Charge (QM/FQ) method,[1,19,26] which was pioneered by Bryce *et al.*[65] There, the environment is described by exploiting a set of charges, which vary as a response to the external potential due to both the other MM atoms and the QM portion. In parallel, FQs polarize the QM density, so that a mutual polarization is established. While the description of the environment in terms of electric charges directly recalls the continuum picture, in FQ the charge transfer between the atoms is governed by the electronegativity equalization principle,[66] which states that, at the equilibrium, the electronegativity of all atoms needs to be the same. Therefore, while continuum approaches are entirely based on electrostatics, the FQ force field finds its theoretical foundations in conceptual density functional theory (CDFT).[67] In fact, it is defined in terms of electronegativities and chemical hardnesses, *i.e.* energy first and second derivatives with respect to the number of particles, which are quantities well-defined in CDFT framework.

The formal similarity of the two approaches, and especially their formulation in terms of electric charges, make the way the energy and molecular properties are formulated very similar. For instance, by taking QM/PCM as an example of continuum solvation approaches, the interaction between the QM and classical portions is expressed as follows:

$$E_{QM/PCM} = \sum_i^{N_\sigma} \sigma_i V[\rho_{QM}](\mathbf{r}_i) \qquad (1)$$

$$E_{QM/FQ} = \sum_i^{N_{FQs}} q_i V[\rho_{QM}](\mathbf{r}_i) \qquad (2)$$

where σ and q are PCM and FQ charges, respectively, and $V[\rho_{QM}](\mathbf{r}_i)$ indicates the electrostatic potential due to the QM density ρ_{QM}, which is calculated at PCM cavity tesserae or FQ atoms positions.[13,19] In fact, while PCM charges are placed at representative points laying on the molecular-shaped cavity, FQ charges are placed at solvent's atomic positions. This introduces a more realistic picture of the environment. The description provided by QM/FQ can be further refined by introducing an explicit treatment of out-of-plane, anistropic interactions. This can be done by including an additional polarization source, which can be expressed for instance in terms of fluctuating dipoles, thus giving rise to the resulting FQFμ force field, which has also been successfully applied to many problems in computational spectroscopy.[40,68,69]

To end this section, it is worth highlighting that a three-layer approach, combining QM/FQ with an outer PCM (spherical) layer (QM/FQ/PCM), has been proposed and extended to the calculation of several spectral signals.[15,70–72] In this case, extensive numerical testing has evidenced little effect of the PCM layer on computed properties/spectra.[73,74] This is mainly due to the fact that in all applications a sufficiently large number of explicit solvent molecules around the solute have been considered. Thus the PCM layer simply results in a sort of confining potential, with only a scarce role in computed values.

Going beyond electrostatic approaches

As stated above, in QM/continuum and QM/atomistic approaches, solute–solvent interactions are generally limited to electrostatic (and polarization) forces. Although such an assumption may be justified for highly polar solvents, non-electrostatic terms (*i.e.* exchange–repulsion, or Pauli Repulsion and dispersion) should be considered to build up a physically consistent modeling.[75,76] These terms, which are generally called van der Waals interactions, are particularly difficult for semi-classical descriptions. In fact, they originate from the quantum nature of the electrons (the Pauli principle, and density fluctuations), and thus have no correspondence in the classical world. A possible strategy is to resort to QM-based approaches, such as QM/Effective Fragment Potential (QM/EFP),[77–79] which however does not belong to the family of QM/classical approaches because it relies on a preliminary full QM calculation on the different moieties constituting the external environment. Indeed, within the framework of QM/classical approaches, *ad hoc* models need to be defined. Some work in this direction has been done for both implicit and explicit modeling, especially for the description of the ground state.[48,50,80–83] Extension of the models to computational

spectroscopy has been only sporadic, although yielding very promising results (*vide infra*).[84–87]

3. How to translate the physics of the system into the modeling of spectral signals in solution

As explained in the previous paragraphs, continuum and atomistic solvation approaches conceptually differ in the way they describe solvent effects on solute's ground state and response properties. The most evident difference is that specific solute–solvent interactions are treated by atomistic descriptions, while they are substantially neglected in implicit models. However, the two modeling strategies have other diverse consequences on the way spectral signals are computed and on the peculiar physico-chemical features that are described.

Conceptually, solvent effects can be categorized as follows:

- Direct effects: the introduction of a solvent-dependent term in the QM/classical Hamiltonian modifies the solute ground state and propagates to spectral properties because solvent contributions also appear in response equations, such as Coupled-Perturbed Hartree–Fock (CPHF) or Kohn–Sham (CPKS) equations, or in the formulation of analytical energy derivatives.[19,26]

- Indirect effects: the solvent modifies minimum geometry(ies). Also, it may change the population of conformers, or give rise to conformations that cannot be accessible in the gas-phase.

The specific formulation of direct effects, *i.e.* the resulting terms entering the equations to be solved, depends on the actual solvation model (either implicit or atomistic) and the QM level that is adopted to describe the solute. Generally, while highly correlated and/or multireference approaches can be fruitfully exploited to study electronic spectra, vibrational, vibronic, magnetic and mixed electric/magnetic spectroscopies are usually computed at the DFT level, which constitutes a good compromise between computational cost and accuracy.[88]

Indirect (geometrical/conformational) effects are instead treated by resorting to different strategies in the two families of methods. In implicit calculations, the minimum geometries are determined through geometry optimization on the solute's potential energy surface (PES) as redefined with the inclusion of solvent-depending terms in the Hamiltonian/energy. Also, the molecular cavity is re-adapted to the diverse geometries that correspond to minima, however the dynamics of the solvation phenomenon (*i.e.* the solvent geometrical rearrangement around the solute) is discarded, giving rise so a substantially "static" picture. Differently, atomistic descriptions require a full configurational sampling of the solute–solvent phase-space, which may be achieved by resorting to classical or *ab initio* molecular dynamics (MDs) simulations, Montecarlo sampling, and other advanced sampling techniques.[89] In this way, the dynamics of the solvent around the solute and their mutual geometrical conformation are taken into account.

Obviously, the description of indirect effects that results from implicit/explicit approaches might be drastically different. Generally, explicit models yield more realistic descriptions, especially in the case of strongly interacting solute–solvent couples, dominated for instance by hydrogen-bonding effects.

The account of indirect solvent effects on spectral properties has relevant consequences from the computational point of view. In fact, implicit approaches follow the same strategies as QM methods for gas phase systems: the calculation of the spectral property is performed on each minimum conformation and then averaged according to Boltzmann populations computed by including solvent effects in the evaluation of (free) energies. Therefore, the cost of the calculation basically stays the same as for isolated systems, if self-consistent-field (SCF) descriptions (HF or DFT) of the QM portion are exploited. A different approach is followed in atomistic simulations. First, limiting the evaluation of the spectral properties on a single structure for each solute conformer surrounded by the solvent placed at specific geometrical positions is unphysical, because realistically the solvent configurations around the solute need to be sampled. For this reason, the spectroscopic signal is calculated on a set of uncorrelated structures taken from the sampling, whose number is selected so as to ensure the convergence of the property. Therefore, while in implicit descriptions the number of calculations equals the number of conformers, atomistic treatments require to evaluate the property of a number of structures that may vary from a few tens to several thousand.[7,15,40] As a consequence, the total computational cost of explicit modeling is roughly n times larger than the corresponding implicit description (where n is the number of snapshots). These two procedures also highlight an important conceptual difference between the two approaches: in atomistic modeling, the average over solute–solvent configurations is explicitly performed, whereas in implicit methods the average is intrinsically considered by the solvent permittivity constant, which is by itself an averaged quantity.

The measured spectrum is the result of the evolution in time of the solute density interacting with the external field, which oscillates within a specific frequency range (UV-Vis, IR, MHz ecc.). This range determines how the spectrum is actually computed at the various QM levels, *i.e.* the formalism and equations that need to be solved. However, the QM theoretical framework needs to be coupled with the solvent evolution in time under the effect of the probing field. In particular, the solvent may only partially follow the solute which evolves under the effect of the field, because some of the solvent degrees of freedom can follow or stay frozen depending on the timescale associated with the solute excitation.

Also, modifications in the external electromagnetic field caused by the presence of the solvent need to be considered. This concept dates back to the Onsager model,[38] where the "local field" is first introduced. In that case, it can be analytically evaluated for both static and dynamic fields, in terms of permittivity constants. In modern implicit solvation schemes, the presence of a molecular-shaped cavity and the description of the solute at full QM level yield local field factors not only

depending on the solvent dielectric properties but also on the solute, and the specific spectral bands.[17,18,90–92] Local field effects have been specified to many response and spectral properties treated by means of implicit solvation models, notably improving the agreement between calculated and experimental values. Much less attention has been paid so far to the formulation of local field effects for atomistic solvation models.[93,94]

3.1 Electronic spectroscopy

The timescales associated with electronic phenomena are of the order of femtoseconds, thus it is reasonable to assume the solute's geometry stays frozen to the ground state – GS (*i.e.* the Frank–Condon approximation) and that the same holds for the solvent nuclear degrees of freedom. Therefore, only the solvent electronic degrees of freedom follow the solute excitation.[13] This means that the system enters the so-called electronic nonequilibrium regime, which is a concept well grounded in implicit solvation, where it is assumed the solvent polarization separates into two parts: a "fast" term accounting for the electronic degrees of freedom of the solvent, which can instantaneously rearrange to the solute's time evolution, and a "slow" contribution, which accounts for the degrees of freedom which remain fixed to the GS, *i.e.* orientational and vibrational. The fast and slow components are represented by two distinct surface charge densities, which are computed using frequency-dependent (fast) or static (slow) dielectric constants.[13,41,95–97]

Differently, in polarizable QM/MM approaches nonequilibrium is automatically described by readjusting the MM polarizable quantities (multiples) to the transition density (we specify here the discussion to TDHF/TDDFT).[20,36,59,94,98] The other solvent degrees of freedom are kept frozen by fixing the geometry of the frames. Methods based on a combination of fixed multipoles and polarizable dipoles (such as Induced Dipoles and AMOEBA) have a clear correspondence with the implicit picture.[56,62,63] In fact, the "fast" degrees of freedom are modeled in terms of polarizable dipoles, which are equilibrated to the transition density, whereas the fixed multipoles represent the "slow" degrees of freedom. These concepts are more subtle in the case of QM/FQ, where static and polarization contributions are calculated together. However, the static contribution can be seen as arising from differences in atomic electronegativities, while the polarization contribution is due to the chemical hardness, which enters the definition of the FQ matrix.[20,99] It is also clear that since in electrostatic embedding the MM multipolar distribution is fixed and does not depend on the QM density, neither nonequilibrium nor direct contributions to response equations are described, thus yielding an unrealistic picture of the electronic excitation.[20]

As stated above, polarizable approaches introduce additional terms in the QM Hamiltonian. When extending the models to the treatment of absorption spectra, it comes out that state-specific and state-average pictures deriving from the linear response formalism in the SCF context, which *in vacuo* coincide, become different. Two complementary formalisms can be exploited,[19,36,57,59,62,98,100–102] depending on which

density the MM polarizable variables are adjusted to. In the linear response (LR) regime, they linearly respond to the transition density,[98,103] while, in state-specific formulations,[104–106] they are adjusted to the excited-state electronic density, for instance by resorting to a first-order correction (corrected linear response – cLR), which has been proposed for both implicit and explicit approaches.[98,103]

From the physical point of view, while in the LR regime dynamic solute–solvent interactions (similar to dispersion interactions) are described, cLR takes into account the relaxation of the solute density in a specific excited state. For this reason, the two formalisms can be seen as complementary and simultaneously considered, such as in the so-called cLR^2 approach.[34,107]

The above discussion assumes the system to be in a nonequilibrium condition. However, once the solvent degrees of freedom fully relax to the solute's excited state electronic density, a novel equilibrium condition arises. This is only achievable if the excited state lifetime is long enough to allow solvent reorganization. Generally, the latter occurs on the order of picoseconds, *i.e.* it is slower than most excited state lifetimes. Solvent reorganization takes place in case of emission phenomena, such as fluorescence. In this case, the solute–solvent couple is at equilibrium in the excited state, and once vertical emission takes place a new nonequilibrium situation arises because the solvent slow degrees of freedom stay fixed to the excited state. In order to consistently describe this phenomenon, implicit approaches resort to geometry optimization (and cavity adjustment) in the excited state geometry.[13] In discrete models, excited state equilibration is much more difficult to describe because the commonly exploited classical methods to sample the phase space are designed for the ground state. To solve this problem, excited state QM/MM MD simulations can be exploited, but their computational cost might become prohibitive. A pragmatical alternative implies the parametrization of classical force fields to properly describe the solute's excited state, however this topic has received so far only a little attention, so established protocols still need to be defined.[108,109]

3.2 Vibrational spectroscopy

Vibrational spectroscopic (*i.e.* Infrared Absorption and Raman scattering) are generally modelled by resorting to the double harmonic approximation, *i.e.* the PES is assumed to be harmonic and intensities are formulated in terms of first derivatives of the dipole moment with respect to normal mode coordinates. From the theoretical point of view, this means that first (gradients) and second energy derivatives (Hessian) with respect to nuclear coordinates need to be evaluated, by resorting to analytical or numerical algorithms. Analytical energy derivatives for implicit (PCM) approaches have been presented,[110–112] by also considering a nonequilibrium response of the solvent to the molecular vibrations and the addition of local field effects in the calculation of IR or Raman intensities.[113] Vibrational nonequilibrium effects are modelled similarly to electronic processes (see Section 3.1), however in

this case the fast component of the solvent polarization adjusts to the electronic and vibrational solute's degrees of freedom. The molecular cavity is also kept fixed to the equilibrium geometry, so to further mimic a nonequilibrium solvation regime.[113,114] Among polarizable QM/MM methods, QM/FQ is the most amply tested to calculate vibrational spectral signals, due to extensive work on the development of analytical derivative algorithms.[69,70,73,74] Other polarizable approaches have been only recently extended to the evaluations of vibrational signals, however their performance has not been extensively tested yet.[69,115]

Within the harmonic approximation, it is assumed that the molecule lies in the PES minimum, which within the focused approach is found by only optimizing the solute's geometry. This corresponds to assuming that the spectral signal is determined by the solute, and only modified by the environment. QM/MM geometries, which as already mentioned above, are obtained from a sampling of the solute–solvent phase-space, are not necessarily associated with energy minima. Consistently with the focused approach, QM/MM vibrational properties are computed by optimizing the solute geometry but keeping the structure of the environment fixed (i.e. the position of solvent molecules).[73,74,116] From the theoretical point of view this procedure complies with the so-called Partial Hessian Vibrational Approach (PHVA),[117] thus only the QM–QM portion of the Hessian matrix is retained, whereas the MM–QM, QM–MM, and MM–MM blocks are discarded.

From the computational point of view, simulating vibrational properties by using QM/MM approaches is more demanding as compared to implicit descriptions. This is mainly due to the fact that the geometries obtained from the sampling might be far from solute minima, and might require a large computational cost (in terms of the number of iterations) to converge. However, the QM/MM description of vibrational spectra that is achieved compares much better with experimental findings, especially in the case of aqueous solutions (vide infra).[1] Notice also that attempts to reduce the computational cost associated with the calculation of the QM/MM Hessian have been recently proposed in different contexts (vibronic and Resonance Raman spectra),[118,119] by projecting out the out-of-equilibrium normal modes, which are generally associated with the flexible dihedral angles. The selection of such modes is far from trivial, therefore it may strongly benefit from novel techniques to automatically select torsional modes.[120]

Finally, it is worth mentioning that specific spectral regions may be dominated by anharmonic effects.[121] However, due to the large computational cost associated with anharmonic calculations, they are generally computed with implicit solvation approaches.[122]

3.3 Magnetic spectroscopy

The strategy that is followed to model magnetic spectroscopies in solution by means of implicit or explicit QM/MM approaches is similar to electronic spectroscopy.[72,123] In fact, formally there is no need to compute spectra on energy minima, therefore

while continuum calculations are performed on PES minima, QM/MM calculations may be performed on structures extracted from the GS sampling, and then averaged, without any further optimization. As for direct solvent effects, also in the case of magnetic perturbations, additional terms arising from the presence of the solvent, need to be considered. In this respect, the presence of a magnetic perturbation acting on a molecular system renders approximated method particularly difficult to be safely applied to the calculation of magnetic properties and spectra, for instance, NMR shieldings or Magnetic Circular Dichroism.[72,123–125] This is not restricted to solvated systems, but of general occurrence, and is due to the fact that the magnetic field, and the associated magnetic vector potential, make the problem origin dependent.[126] The Gauge Independent Atomic Orbitals (GIAOs) have been introduced to solve this problem.[127] The extension of polarizable implicit or explicit models to magnetic perturbations requires introducing additional contributions as compared to electric perturbations, due to the use of GIAOs, as shown in ref. 72, 123 and 128. In addition, it is worth noting that the perturbed polarizable variables, in case of a magnetic perturbation, would be imaginary, similarly to the perturbed density. This is conceptually in contradiction with the semiclassical nature of QM/classical models, therefore such variables are not considered in theoretical formulations. Similarly, in the calculation of NMR shieldings explicit polarizable classical contributions are not included, thus their dependence on the nuclear magnetic moment is not considered. Also, the external magnetic field is formally static, then oscillations in the solvent electronic density (i.e. nonequilibrium effects) are not included in any description, whereas, as usual, solvent fluctuations are introduced in atomistic approaches.

It is also worth remarking that in either QM/continuum or QM/atomistic descriptions, the interaction between the QM and the classical portion is retained as purely electrostatic (see also eqn (1) and (2)). Non-electrostatic interactions (exchange, repulsion, dispersion) are generally discarded. However, while this assumption is reasonable for electric perturbations, it is much less justified for magnetic perturbations, where density fluctuation and confinement may play a relevant role up to generate induced densities in the environment. To the best of our knowledge, such effects have only marginally been taken into account in QM/classical approaches. As for QM/FQ, it has recently been challenged to describe EPR hyperfine coupling constants with the inclusion of no-electrostatic solute–solvent interactions,[83] however full extension to magnetic properties and extensive testing are still missing.

3.4 Mixed electronic/vibrational/magnetic spectroscopy

The last class of spectroscopies that we treat in this perspective arises from the combination of electronic/vibrational degrees of freedom and electric/or magnetic spectral responses. From the theoretical point of view, these are intrinsically more complex, because involve various degrees of freedom at the same time, each of them associated with a specific time-scale that needs to be coherently coupled to the solvent's time and

spatial evolution. To further explain this concept, we take as an example Resonance Raman (RR) spectroscopy.[129] There, differently from far-from-resonance Raman spectra, the external laser frequency coincides with a solute electronic excitation band, thus yielding a substantial enhancement of selected vibrational modes. The peculiar nature of RR, which is formally a mixed vibrational–electronic property, calls for care when coupled to solvent time evolution. Only a few works have attempted a systematic approach to describe this phenomenon at the QM/PCM level properly.[130–133] Only recently, the polarizable QM/FQ approach has been extended to this property.[8,134,135]

RR signals and the environment are so tightly connected that RR is often exploited to evaluate solvent reorganization energies following electronic transitions.[136] The presence of the solvent influences the positions of the peaks, which are related to modifications in vibrational energies, which in turn follow from changes in the PES. Therefore, reliable computational protocols need to be able to model at the same time and with similar accuracy the effects of the solvent on electronic transition energies, geometries, frequencies, and vibrational wave functions. Clearly, this means that solvent terms enter the calculation of the molecular electronic wave function, and alter the solute PES, *i.e.* equilibrium geometries, vibrational frequencies, and normal modes. Also, solvent terms need to be included in the evaluation of the excited state properties which are required to evaluate RR spectral intensities, *i.e.*, transition dipole moments, excited state forces, and possibly Hessian, depending on the theoretical level which is exploited to describe RR signals.[131]

Within the implicit solvation framework, the nature of RR as a mixed vibrational–electronic spectroscopy calls for care when considering the solvent time evolution, in order to correctly account for the dynamical aspects of the solute–solvent interaction. The RR polarizability, which rules spectral intensities, originates from the time evolution of a vibrational wave packet on the excited state PES. Depending on the time scale of such an evolution, some of the solvent's nuclear degrees of freedom may remain static. A possible way to simulate this regime with implicit modeling in an approximate way (see ref. 137 for more details) consists of keeping the molecular cavity fixed to the solute GS equilibrium geometry and model normal models and frequencies within the vibrational nonequilibrium regime. The (electronic) nonequilibrium excitation energy derivative is then computed by also keeping the cavity fixed. Generally speaking, univocal assessment of the correct (nuclear + electronic) solvation regime in modeling RR spectra is not straightforward. Different combinations have been tested in ref. 137 leading to considerable differences in computed spectra. In addition, the solute–solvent interaction term acting on the RR polarizability is modeled by considering a dephasing term that can no longer be attributed solely to the finite lifetime of the molecular excited electronic state but should take into account the experimental conditions.[137] The above discussion should have highlighted the complexity of RR signals, and their consequences on the computational approach. Clearly, in order to

properly simulate RR of solvated systems by means of an explicit (polarizable) QM/MM approach, the latter needs to be able to tackle at the same time and with the same level of accuracy, the GS electronic and vibrational degrees of freedom of the system, as well as its excited states. Remarkably, QM/FQ has such features, therefore it has recently been successfully applied to the calculation of RR.[8,134,135] Due to the full atomistic nature of the model, nonequilibrium effects are automatically considered by the computational protocol, in line with what has been discussed in Section 3.1 for electronic spectra.

Chiroptical spectroscopies are another fascinating class of mixed electric, magnetic and/or vibrational responses.[138] Examples are Electronic Circular Dichroism (ECD), Optical Rotation (OR), Vibrational Circular Dichroism (VCD) and Raman Optical Activity (ROA).[138–140] These kinds of spectroscopies are generally exploited to assign the absolute configuration of chiral molecules, especially molecular drugs, and for this purpose need to be assisted by molecular simulations.[26,141,142] The effect of the solvent on the measured signal can be drastic, *i.e.* the solvent can even change the sign of the measured properties or the sign of specific bands with respect to simulations for the isolated systems.[26,72] Such complexity comes together with the complexity of the signals to be simulated, which require the simultaneous consideration of electronic and magnetic perturbations, further coupled to geometrical perturbations for VCD/ROA.[139] Also, all perturbations need to be treated at the same level of accuracy, to avoid unphysical descriptions. While QM/PCM has been extended to the analytical evaluation of all aforementioned chiroptical properties and spectroscopies,[143–145] to the best of our knowledge QM/FQ is the only polarizable QM/MM method able to treat all these signals, remarkably through analytical algorithms.[19,73,74,116]

The strategy to model chiral spectra derives from the nature of the spectral signal. In fact, in the case of ECD, the theoretical framework does not require the calculation of spectra on energy minima, therefore the same strategy followed for purely electronic or magnetic spectroscopies can be exploited.[91,146] This again means that continuum calculations are generally performed on GS PES minima, whereas QM/MM ECD calculations may be performed on structures extracted from the GS sampling without any further optimization.[147,148] As for direct solvent effects, additional terms arising from the presence of the solvent need to be considered in the calculation of the response tensors to the presence of the external circularly polarized light, by simultaneously taking into account the electric and magnetic components. Also, the description of solvent nonequilibrium is the same as electronic absorption spectroscopy, then follows the same strategies discussed in Section 3.1.[91]

Moving to VCD or ROA, the spectral signal arises from the interaction of the polarized light (electric and magnetic components) with the vibrational degrees of freedom of the molecule, which lies on the GS. Therefore, the same consideration as IR and Raman spectra hold. Then, to comply with the harmonic approximation, it is necessary for the calculations to be performed on PES minima. Reaction and local field effects need

also to be included in the calculation of QM/PCM VCD and ROA tensors, as well as a proper description of solvent vibrational nonequilibrium effects, similar to what is discussed in Section 3.2.[73,116,144,145]

4. Illustrating the concepts

In the following, the performance of both implicit and explicit approaches is illustrated for the various spectral signals discussed above. We have selected specific cases in which the differences between the two approaches are particularly marked. Most reported values refer to aqueous solutions, which among the many characteristics that make them unique, feature strong solute–solvent interactions through hydrogen bonding.

Before deepening the discussion of the selected examples, it is worth pointing out that continuum solvation models are nowadays available in most quantum chemistry software, both commercial and open-source, so that various kinds of spectra can be computed in a plethora of solvents. Open-source libraries, such as PCMSolver,[149] are also freely available and interfaced with many codes. Unfortunately, the same does not hold for polarizable QM/MM approaches, which are only sporadically included in quantum chemistry codes or in open-source libraries.[150] Most implementations, however, are limited to a single specific force field, thus limiting wide applicability. A remarkable exception is ADF[151,152] which is part of the Amsterdam Modeling Suite (AMS),[153] where three different polarizable force fields, either based on FQ or induced dipoles[63] are available and extended to several kinds of spectra, thus allowing for a consistent comparison between the various approaches.[40] Also, the current implementation in ADF, and the related graphical interface, guide the user along the whole computational protocol which needs to be followed to perform (polarizable) QM/MM spectral calculations.[154]

4.1 UV-Vis absorption and emission spectra

As the first example to illustrate the modeling of UV-Vis absorption spectra of solvated systems, we select betaine (BET, see Fig. 1a)), which features large solvatochromic shifts when dissolved in different solvents and has been used to develop the popular Reichardt's polarity scale based on ET(30).[155] Thanks to its peculiar electronic properties, BET is an ideal playground to quantitatively and qualitatively appreciate the differences between explicit and implicit solvent descriptions.

In ref. 34, BET absorption spectrum has been computed at the QM/PCM, QM/EE and QM/FQ levels of theory, as dissolved in dioxane (DIO, polarity index $\phi = 0.164$), acetonitrile (ACN, $\phi = 0.460$), methanol (MET, $\phi = 0.762$) and water (WTR, $\phi = 1.000$). The solvent polarity scale ϕ is defined in terms of the solvatochromic shift exhibited by BET lowest $\pi \rightarrow \pi^*$ electronic excitation, which has a charge-transfer character (see Fig. 1a). In Fig. 1b, computed and experimental[156,157] absorption energies as a function of the solvent polarity are graphically
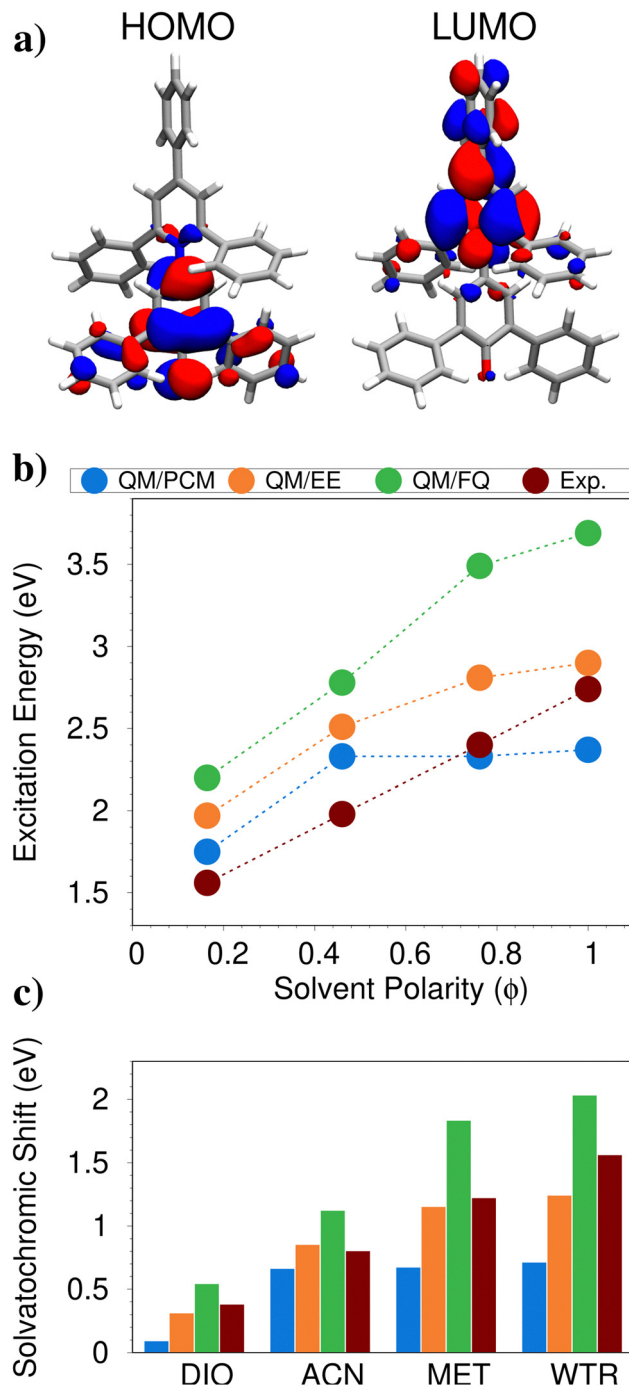

Fig. 1 (a) Graphical depiction of BET HOMO and LUMO in aqueous solution. (b) Experimental and computed QM/PCM, QM/EE, QM/FQ absorption energies as a function of solvent polarity ϕ. (c) Experimental and computed QM/PCM, QM/EE, QM/FQ solvatochromic shifts with respect to the *in vacuo* absorption (experimental: 1.66 eV; computed: 1.18 eV). QM level: CAM-B3LYP/6-31+G*. Figure reproduced from ref. 34.

depicted. Among the tested computational approaches, the polarizable atomistic QM/FQ is the only one that is able to reproduce the experimental behavior, while both the non-polarizable QM/EE and the implicit QM/PCM values flatten out as the solvent polarity increases. The differences between

the tested methods can be further appreciated by comparing solvatochromic shifts, *i.e.* the differences between the absorption maxima in solution and in gas-phase (see Fig. 1c). First, we note that QM/PCM cannot correctly reproduce the experimental solvatochromic shifts for the most polar and protic solvents. The non-polarizable QM/EE, instead, gives values that are in very good agreement with the reference data, in particular for DIO, ACN and MET. The polarizable QM/FQ approach predicts solvatochromic shifts which are generally larger than experiments. However, it is worth noting that all approaches limit the QM-classical interaction to purely electrostatic forces. However, solute–solvent Pauli repulsion can play a relevant role, providing quantum confinement in the electronic density. For instance, if these effects are taken into account (for instance by using the approach developed by the authors in ref. 80), for aqueous BET the estimated error moves from 0.46 eV to 0.1 eV, overall reducing computed solvatochromic shifts. Therefore, the QM/EE good performance reported above is probably caused by error cancellation, due to the fact that both Pauli repulsion and solute–solvent polarization effects are neglected. Notice that very good agreement between computed and experimental values is also reported by the polarizable method exploited in ref. 62, which is based on a multipolar expansion of the QM/MM interaction.

Similar outcomes result from the study of the n → π* transition of pyrimidine (see Fig. 2a), which is a rather rigid molecule.[98,158–161] In this case, the values are averaged over 200 snapshots that have been extracted from MD simulations where pyrimidine is kept fixed to the QM/PCM optimized geometry. In this case, we focus simply on vacuo-to-water solvatochromic shifts, as computed by using purely implicit QM/PCM or explicit polarizable QM/FQ and non-polarizable QM/EE approaches. From the inspection of Fig. 2b, it is clear that while QM/PCM cannot reproduce the experimental reference values, QM/EE apparently yields solvatochromic shifts in agreement with experiments. Similarly to the previous case, the polarizable QM/FQ, instead, overestimates, in absolute value, the experimental solvatochromic shift. However, an almost perfect agreement is obtained if Pauli repulsion effects are included. Indeed, quantum confinement has a drastic effect on calculated solvatochromic shifts, affecting the data by about 30/40% on average.

It is worth remarking that a systematic study on the computational prediction of vacuo-to-water solvatochromic shifts by exploiting both non-polarizable QM/EE, and polarizable QM/FQ, QM/FQFμ, QM/DRF (fixed charges and induced dipoles in the MM portion) has recently been proposed.[40] The results reveal that none of the approaches outperform the others and that errors strongly depend on the nature of the molecular transition to be described, thus highlighting that the description of solvatochromic shifts is indeed a delicate task.

To conclude the discussion on electronic spectra, we focus on the fluorescence spectrum of acetone in an aqueous solution, which is an illustrative example of the complexity associated with emission phenomena. Although acetone is a rather small molecule, in aqueous solution it undergoes a
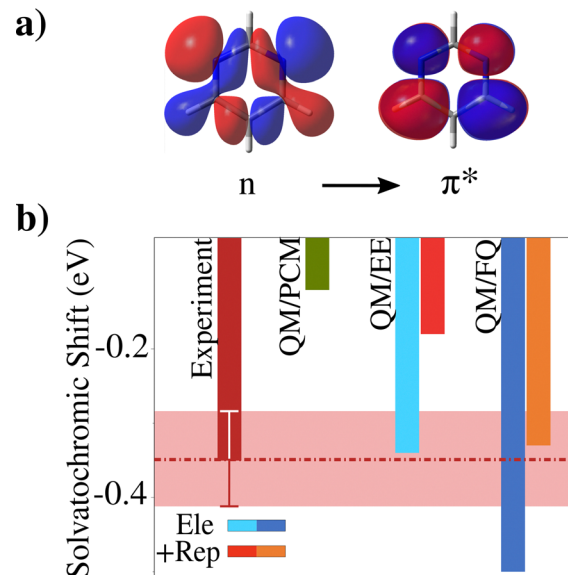

Fig. 2 Pyrimidine experimental and computed QM/PCM, QM/EE and QM/FQ vacuo-to-water solvatochromic shifts. For QM/MM, the results obtained by including solute−solvent Pauli repulsion are also given (+Rep). Reference gas-phase vertical excitation energies: 4.17 eV (calculated); 4.18 ± 0.01 eV (experimental). The red shadowed region indicates the experimental error bar. QM level: M06/6-311+G(2df,2p).

geometrical distortion in its first excited state geometry (see Fig. 3), which is associated with a n → π* transition. In fact, while in the ground state, the improper dihedral angle δ oscillates around 0 degrees, in the excited state, the geometry is distorted and δ oscillates between ±20 degrees. Therefore, to properly predict the fluorescence spectrum of aqueous acetone, the solute–solvent phase-space in the excited state needs to be accurately sampled. To this end, classical MD simulations can be exploited, however they need to be based on force fields that are suitably refined to reproduce ES energies, gradients, and Hessian, together with a correct accounting for changes in the solute electronic density.

The emission solvatochromic shifts associated with the π* → n transition of acetone in aqueous solution as calculated at the QM/PCM and QM/FQ levels are graphically reported in Fig. 3. QM/FQ values are obtained by averaging over a set of uncorrelated snapshots extracted from classical MD simulations. Effects of Pauli repulsion contributions are also considered for QM/FQ (+Rep) again by means of the method proposed by the authors in ref. 80. Indeed, repulsive interactions affect the averaged QM/FQ emission energy, thus yielding a final computed shift of about ∼−0.01 eV. This value is in almost perfect agreement with the experimental shift (see Fig. 3), showing that QM/FQ + rep is the only method that can model the experimental negative solvatochromic shift. Remarkably, a positive shift is reported instead by both QM/FQ and QM/PCM.

4.2 Infrared absorption and Raman spectra

To showcase the performance of polarizable implicit *vs.* explicit solvation modeling on vibrational spectroscopy, we focus on
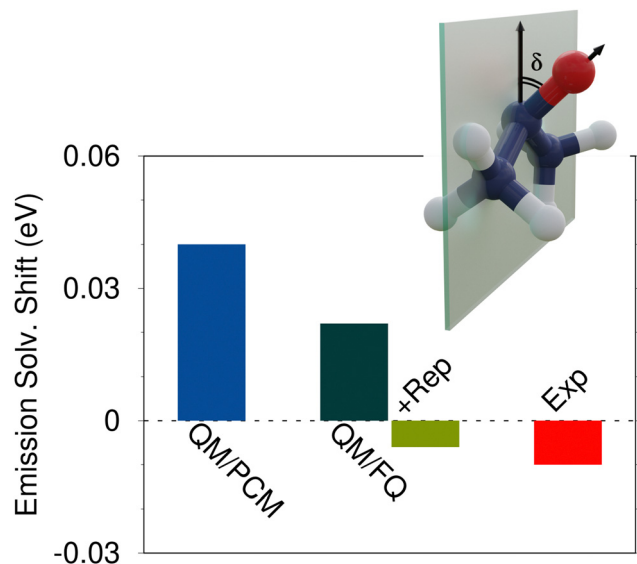
Fig. 3 Experimental and computed QM/PCM, QM/FQ and QM/FQ + rep emission vacuo-to-water solvatochromic shifts for acetone in aqueous solution (see also ref. 108). QM level: CAM-B3LYP/aug-cc-pVDZ.

Fig. 4 Experimental[162] and calculated QM/PCM, QM/FQ and QM/FQFμ IR spectra of gallic acid in aqueous solution (QM/PCM FWHM = 10 cm^{-1}; QM/MM FWHM = 4 cm^{-1}). QM/PCM, QM/FQ and QM/FQFμ stick spectra are also depicted as grey lines. QM level: B3LYP/6-311++G**.

the IR spectrum of gallic acid in aqueous solution (see Fig. 4). In this case, the description provided by QM/FQ is further refined by including an additional polarization source defined in terms of fluctuating dipoles (Fμ). The resulting method is called QM/FQFμ.[68] As discussed above, QM/FQ(Fμ) spectra are obtained by averaging the results over a set of uncorrelated snapshots extracted from classical MD simulations (in this case 200 snapshots).[69] Raw data extracted from QM/PCM, QM/FQ and QM/FQFμ calculations on each snapshot are reported as sticks (grey lines) in Fig. 4. Final spectra are generated by convoluting each stick with a Lorentzian band shape (full with at half maximum – FWHM of 10 or 4 cm^{-1} for QM/PCM and QM/MM spectra, respectively). Both atomistic approaches can estimate band inhomogeneous broadening, which arises from the large variability in both stick frequencies and intensities. Remarkably, this results from the dynamic picture of the solvation phenomenon which is modelled by these methods when combined with the explicit sampling of the phase-space, achieved in this case by means of MD simulations. Differently, in the static QM/PCM approach band broadening is only artificially added, and it is homogeneous by definition. In fact, each peak visible in the final spectrum is due to a specific vibrational normal mode of the solute.

The quality of the reproduction of experimental data[163] is also different for the two approaches. In fact, the experimental spectrum is characterized by three bands in the region 1200–1500 cm^{-1}, which involve a combination of different normal modes, and by the presence of a well-separated peak at 1000 cm^{-1} (C–OH bending) and three low-in-intensity bands (1500–1800 cm^{-1}), that are associated to composite C–OH bending modes of the hydroxyl groups and the acidic C=O stretching. While the general features of the experimental spectrum are generally reproduced by all solvation models,
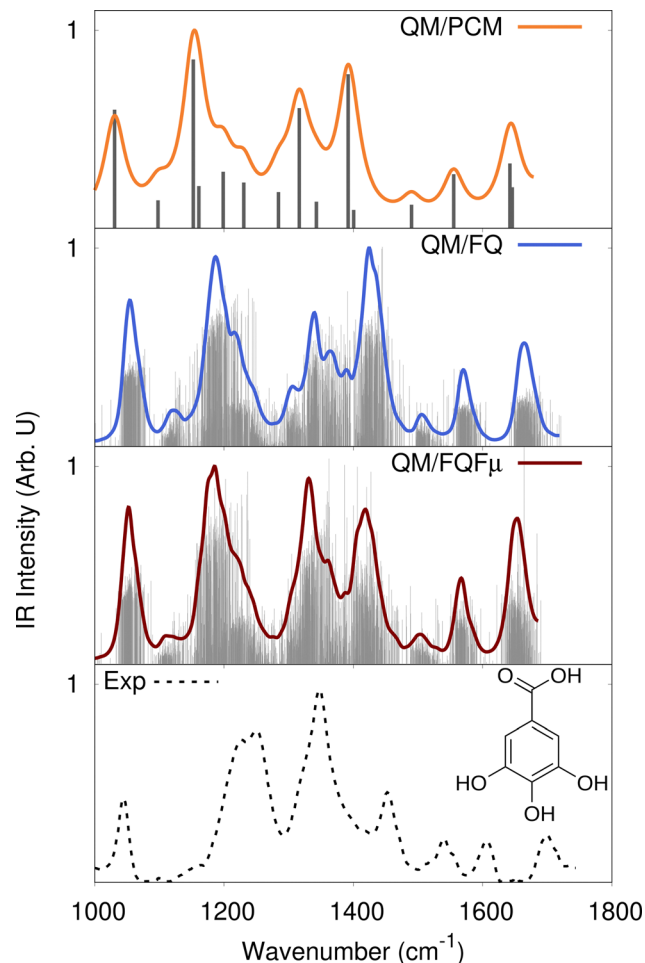
the intensity of the band at about 1350 cm^{-1} (the most intense in the experimental spectrum) is correctly predicted only by QM/FQFμ. Remarkably, it is interesting to note that as it is reported in ref. 162, the intensity of this peak is correctly reproduced by exploiting a supermolecule approach, where 8 water molecules are included in the QM region in QM/PCM calculations. Therefore, specific and non-electrostatic interactions probably play a substantial role in this spectral region, therefore purely electrostatic approaches, such as QM/PCM, QM/FQ and QM/FQFμ cannot perfectly reproduce the experimental findings. Finally, the inhomogeneous band broadening that is predicted by both atomistic approaches is in very good agreement with the experimental data, in particular for the patterns in the spectral region between 1200 and 1400 cm^{-1}.

As an additional example, we move to the vibrational absorption spectrum of methyl-lactate (MLac) in aqueous solution.[74] QM/PCM predict three main conformations (see red dots in Fig. 5b),[74,164] as a consequence of the flexibility of the dihedral angles δ_1 and δ_2 (see Fig. 5a). A completely different conformational distribution arises from MD simulations (see Fig. 5b).
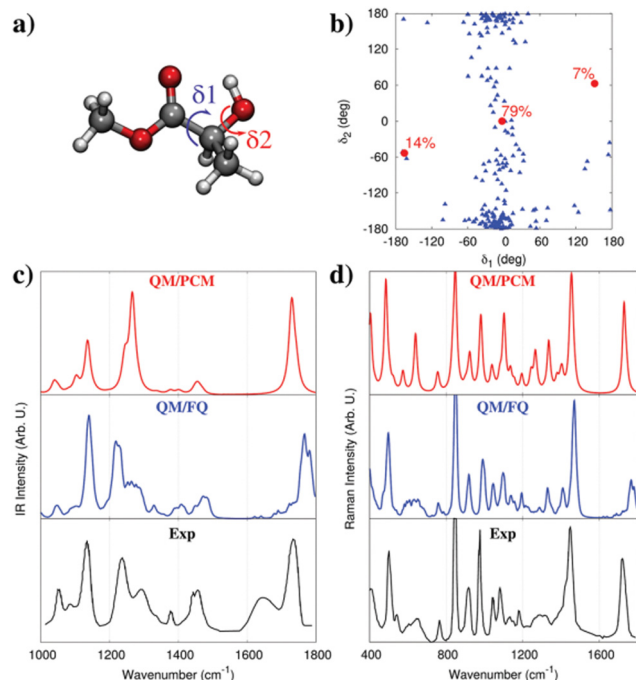
Fig. 5 (a) MLac molecular structure. δ_1 and δ_2 dihedral angles are also highlighted. (b) MD population map as a function of δ_1 and δ_2 (blue triangles). The three QM/PCM conformations (red circles) and their populations are also given. (c and d) Experimental[164,165] and computed QM/PCM and QM/FQ IR (c) and Raman (d, 488 nm) spectra of aqueous MLac (see also ref. 74). QM level: B3LYP/aug-cc-pVDZ. Figure is reproduced from ref. 1.

In fact, MLac tends to cluster around a conformer, which is however absent in the QM/PCM conformational analysis. Such a difference is due to the formation of hydrogen bonding interactions between MLac and water in MD simulation, whereas QM/PCM structures are mainly characterized by intra-molecular hydrogen bonding, due to the absence of explicit solvent molecules in the PCM description. The resulting MLac IR and Raman spectra can be compared with the experiments. By first considering the IR spectrum (Fig. 5c, we note that QM/PCM and QM/FQ yield a completely different description of band relative intensities and broadening. The region between 1200–1300 cm^{-1}, which involves OH group vibrational motions, is almost perfectly reproduced by QM/FQ. On the contrary, the QM/PCM spectrum is characterized by an intensity pattern that disagrees with the experimental spectrum. Similar findings also apply to the Raman spectrum (see Fig. 5d), for which QM/PCM and QM/FQ predict different relative intensity patterns, especially in the region between 1200–1300 cm^{-1}. This confirms once more the benefit of atomistic descriptions of the environment.

4.3 NMR shieldings

To show the different descriptions of solvent effects on magnetic properties provided by implicit and explicit models, we select the NMR shieldings of pyrimidine as dissolved in aqueous solution.[72,166] For this particular system, it has been shown that a minimal model of solvation, constituted by the

molecule and two H-bonded water molecules, provides similar results to that obtained by using a dynamical sampling by means of a classical MD simulation.[72] It is worth noting that this is not generally true, and indeed a static minimal picture provided by a cluster approach generally fails at reproducing solvent effects.[1] The minimal structure, belonging to the C2v point group, exploited in ref. 72 is reported in Fig. 6a. NMR shieldings are calculated by describing the solvent at the PCM level (QM/PCM), or by treating the two H-bonded water molecules either at the full QM level (QM/QMw) or classically, by means of FQ (QM/FQ). In the resulting cluster model, long-range effects have also been considered by surrounding the minimal system with a third PCM layer (QM/QMw/PCM and QM/FQ/PCM).

Among the different representations of solvent effects, QM/QMw/PCM can be considered the most accurate and can be taken as a reference, because all interactions between the solute and the two water molecules are retained at the QM level. To quantitatively evaluate solvent effects, solvent-induced shifts as compared to gas-phase results are analyzed
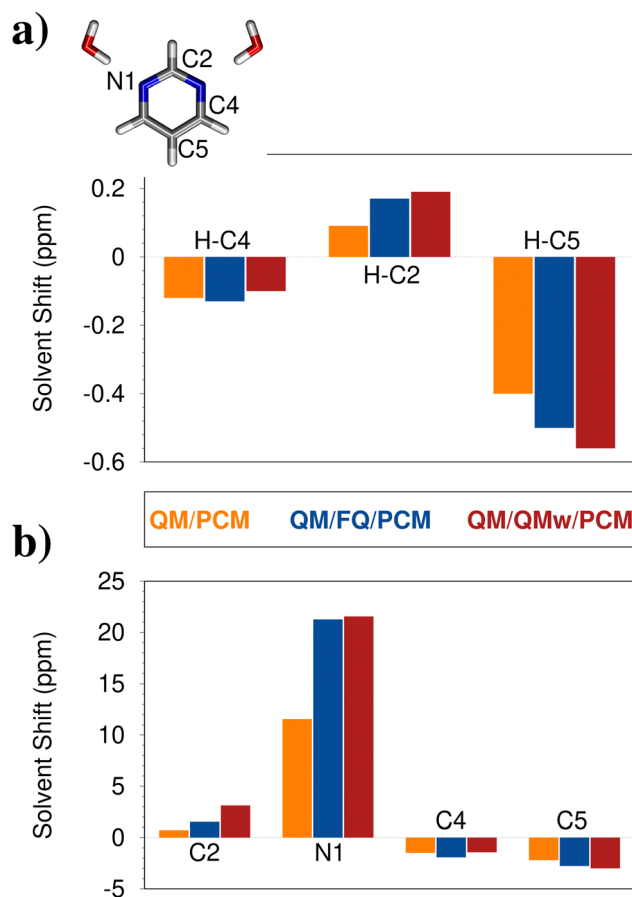

Fig. 6 Computed QM/PCM, QM/FQ/PCM, and QM/QMw/PCM solvent-induced shifts on chemical shifts (ppm) for pyrimidine in aqueous solutions.[72] Values for hydrogen (a) and heavy (b) atoms are shown (only non-equivalent atoms are considered). Chemical shifts are computed on the minimal cluster depicted in panel (a). QM level: B3LYP/6-311++G(2df,2pd)

and graphically depicted in Fig. 6a and b for hydrogen and heavy atoms, respectively. While solvent has a minor impact on both hydrogen and carbon atoms, it increases the shielding of the nitrogen atom by about 30%. This is not surprising considering that the two explicit water molecules are hydrogen bonded to pyrimidine through the nitrogen atom. Also, QM/FQ/PCM behaves particularly well as compared to the QM/QMw/PCM reference, reporting a root mean square error (RMS) of just 0.4 ppm. Differently, QM/PCM predicts an RMS of 15.2 ppm. Such an error primarily arises from the wrong prediction of the NMR shielding for nitrogen atoms (Fig. 6b), which are instead almost perfectly described by QM/FQ/PCM (the deviation is of just 0.3 ppm). Such findings confirm the benefit of atomistic descriptions to accurately describe hydrogen-bonded systems. To end the discussion, computed solvent shifts can be compared to experimental data. Notice that experimental reference data for calculating solvent shifts are reported for a cyclohexane solution (*i.e.* not for the isolated molecule), which can be reasonably described by means of QM/PCM,[166] due to the absence of strong/specific solute–solvent interactions. The agreement with the experimental value reported in ref. 167 for nitrogen (16.84 ppm) is particularly good (12.73 ppm), especially considering that in our modeling solute–solvent interactions are limited to the electrostatic component, while, as explained in Section 3.3, non-electrostatic forces are expected to play a relevant role in magnetic properties.

4.4 Resonance Raman spectroscopy

As stated in Section 3.4, Resonance Raman (RR) spectroscopy is among the most sensitive to the solvent. As a representative case study, we select *N*-methyl acetamide (NMA), which is often exploited as a prototype model for the peptide bond (see Fig. 7). First, we focus our attention on the Raman spectrum in the far-from-resonance regime, *i.e.* the one which is measured by irradiating the sample at a wavelength that is far from the solute's electronic transitions (633 nm in this case). QM/PCM and QM/FQ spectra are reported in Fig. 7a, together with experimental data. The most significant patterns in the experimental spectrum are the amide I (1626–1646 cm^{-1}), amide II (1566–1584 cm^{-1}), and amide III (1313 cm^{-1})[168] bands. Both QM/PCM and QM/FQ reproduce well the experimental trends, with QM/FQ slightly improving QM/PCM results, especially for the strong amide bands. Also, all QM/FQ bands are generally broader than QM/PCM ones, due to the dispersion in both vibrational energies and intensities, which is obtained as a result of the combination of QM/FQ with classical MD simulations to sample the phase-space. QM/PCM, QM/FQ, and experimental RR spectra of aqueous NMA are reported in Fig. 7b. It is worth noting that the experimental wavelength (226 nm) differs from that exploited in the calculations, because the latter needs to reproduce the experimental conditions in order to have the same resonance enhancement, *i.e.* needs to be close to a computed electronic transition. The comparison between RR and far-from-resonance Raman spectra (see Fig. 7a and b) shows significant differences. In fact, the Amide I (C=O) stretching vibration (1626–1646 cm^{-1}) is weaker, the signal involving the Amide II C–N stretching (1566–1584 cm^{-1}) is enhanced, as also the CH$_3$ umbrella bending (1380 cm^{-1}) band. In addition, the Amide III band (1313 cm^{-1}) gains intensity with respect to Amide I.[169–171] All the aforementioned spectral features are correctly reproduced by QM/FQ, for which the computed spectrum almost perfectly resembles the experiment. A completely different situation results from QM/PCM calculations. In fact, the Amide I band is the strongest in the QM/PCM spectrum. Also, the methyl modes (peak erroneously emerging at 1440 cm^{-1}) are enhanced. Such findings also reveal that
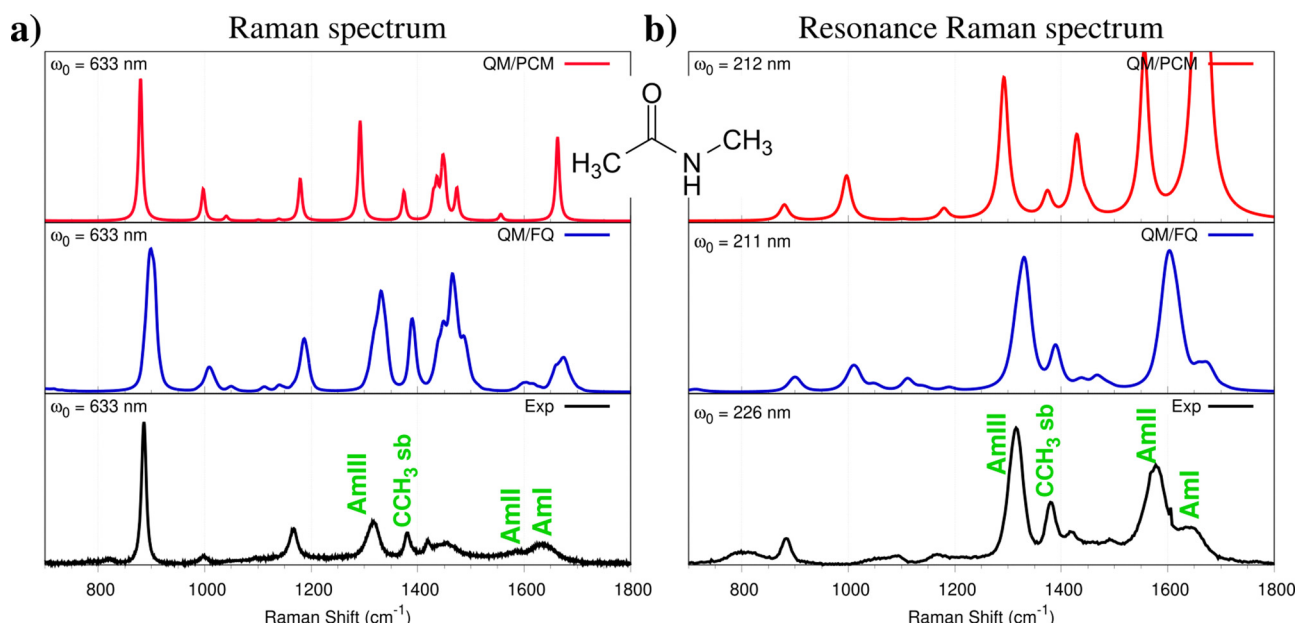

Fig. 7 Experimental and computed QM/PCM, QM/FQ Raman (a) and Resonance Raman (b) spectra of NMA dissolved in aqueous solution. QM level: B3LYP/aug-cc-pVDZ. Figure is adapted from ref. 8.

QM/FQ is notably able to account for the almost threefold enhancement of Amide II with respect to Amide I band, which is experimentally measured. The discrepancies between QM/PCM and experimental spectra, together with the almost perfect agreement provided by QM/FQ, clearly demonstrate the importance of specific solute–solvent interactions, coupled with a physically consistent treatment of polarization effects.

4.5 Chiroptical properties and spectroscopies

Chiroptical properties and spectroscopies are another class of signals which are particularly sensitive to the external environment.[172] One of the most famous examples is the optical rotation (OR) of (R)-methyloxirane (MOXY), which changes sign by moving from the gas phase to the aqueous solution.[173] This has a dramatic consequence: comparison between experimental values and theoretical models which cannot predict the correct sign would result in the wrong assignment of the absolute configuration. This is the case of QM/PCM, which indeed provides a computed sign for aqueous MOXY which is incorrect (see Fig. 8b). The correct sign is described by QM/FQ/PCM, in which an outer third PCM layer is included (at a distance 13.5 Å from MOXY). Indeed, the absolute value of the electronic contribution to OR is underestimated if compared to the experimental value. Due to the high computational cost associated with the calculation of vibrational contributions to OR within a QM/MM scheme, they can be approximated by taking the QM/PCM values (with vibrational nonequilibrium effects) as a ref. 15. When they are included in the average value, not only a qualitative but also a quantitative agreement with the experimental value is achieved.

The final QM/FQ/PCM value is obtained by averaging computed values on a number of snapshots extracted from MD simulations. Differently from the spectral properties mentioned in the previous sections, where a few hundred snapshots guarantee the convergence of the average property, for OR 2000 frames are necessary, thus clearly increasing the computational cost as compared to the static QM/PCM calculation, which only requires a single calculation (R-MOXY features only a single minimum conformation in the PCM PES). The above discussion clearly highlights the complexity of modeling OR, especially when the solute is dissolved in strongly interacting environments, such as aqueous solutions. This can be further appreciated by observing the QM/FQ raw data associated with OR calculations on the single snapshots extracted from the MD simulation (see Fig. 8a). It is evident that not only does the magnitude of the computed OR vary as a function of the considered frame (oscillating between 100 and −100 degrees, while the average falls around −1.2 degrees), but also the sign. The success of the atomistic QM/FQ/PCM approach is the result of the accurate modeling of the physico-chemical features which dominate this property, which are in this case hydrogen bonding interactions and dynamic solvation effects. Similar findings have been reported in ref. 174, where the closest water molecules are included in the QM region, at a much larger computational cost.
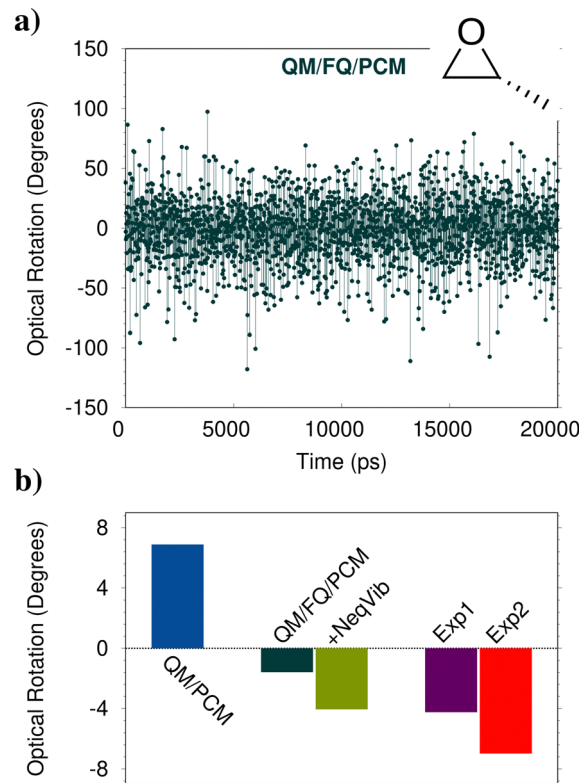

Fig. 8 (a) Computed QM/FQ/PCM OR (589 nm) for aqueous (R)-MOXY as a function of time (MD snapshot). (b) Computed QM/PCM and average QM/FQ/PCM OR at 589 nm of aqueous (R)-MOXY. Vibrational corrections computed at the QM/PCM level with the inclusion of vibrational nonequilibrium effects are also added to QM/FQ/PCM results (+NeqVib). Experimental data reproduced from ref. 175 (Exp1) and ref. 173 (Exp2) are also reported.

To further demonstrate how sensitive chiroptical spectroscopies are to the external environment, we report the case of the Vibrational Circular Dichroism (VCD) spectrum of zwitterionic (L)-alanine (ALA) in aqueous solution.[116,176] As stated above, VCD is the chiral analogous of the IR spectrum and is obtained by irradiating the sample with left and right circularly polarized light; the spectrum results from the difference between the absorption of the two radiations in the infrared region.[140] Alanine experimental VCD spectrum is characterized by a significant (+, −, +) pattern in the region between 1250 and 1450 cm^{-1}. The three bands are associated to normal modes which involve the symmetric stretching of the CO_2^- group and the orthogonal methine CH bending mode. QM/FQ/PCM rotational strengths calculated for each snapshot are reported in Fig. 9, middle panel: a very large variability, in both sign and magnitude, is clearly reported, in line with what has been commented above for MOXY OR. This highlights once more the difficulties related to the prediction of chiroptical spectra of systems embedded in aqueous solution. Similar to the gallic acid IR spectrum, also in this case QM/PCM features much poorer spectral details (see Fig. 9, top panel).

As a result, the static QM/PCM and the dynamic QM/FQ/PCM predict completely different spectra, also with regard to
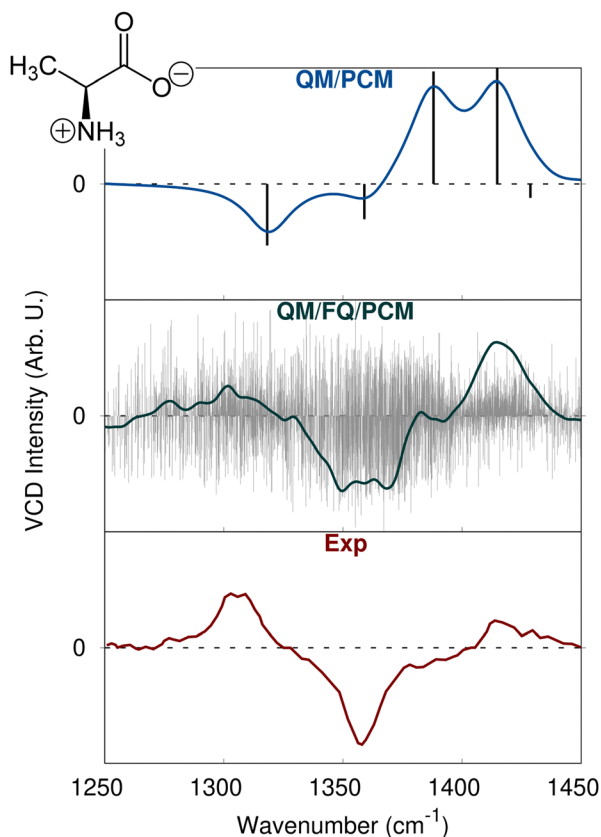
Fig. 9 QM/PCM (blue), QM/FQ/PCM (dark green) and experimental (red)[176] VCD spectra of aqueous (L)-alanine. QM/PCM and QM/FQ/PCM raw spectra are also plotted as grey lines. QM level: B3LYP/6-311++G**.

sign alternation patterns (see Fig. 9). In fact, QM/PCM fails at reproducing the experimental sign pattern, reporting a $(-, -, +, +)$ sign alternation which is not compatible with the experimental spectrum of the L enantiomer. On the other hand, the agreement between QM/FQ/PCM and experimental data is almost perfect and indeed particularly impressive if compared to QM/PCM data. The only slight disagreement between QM/FQ/PCM and experimental spectra stays in the relative intensities of the bands in the region between 1300 and 1500 cm^{-1}. However, the sign is correctly reproduced. It is finally worth pointing out that the dissimilarities between the implicit and explicit descriptions in the prediction of VCD spectra, not only arise from the diverse accounting of the solvent effects on the spectroscopic signal but are also the consequence of explicit solvent effects on the molecular geometry, which is in this case reoptimized to comply with the harmonic approximation.

5. Conclusions

In this feature article we have discussed, from the theoretical and computational points of view, continuum and atomistic solvation approaches to the calculation of molecular spectra. In particular, we have focused on how to translate the physico-chemical features of the molecule/solvent/radiation system into accurate models, which can provide reliable results that can be directly compared with experimental data, and assist their interpretation, in a truly synergistic way. From the chemical perspective, atomistic approaches are much more intuitive as compared to continuum descriptions, because all the atoms of the system are explicitly treated. However, fully atomistic modeling results in more complex (and expensive) computational protocols as compared to modern QM/continuum implementations. Generally speaking, the cost of a single polarizable QM/MM calculation is the same as a single QM/continuum calculation at the same QM level. However, while continuum approaches require a number of calculations equal to the number of conformers, explicit modeling involves as many calculations as those needed to reach convergence in the final spectrum. This number may vary from a few hundred to several thousand, depending on the spectral property and the nature of the interaction between the solute and the solvent. As a consequence, QM/continuum approaches are generally worth a try, by however keeping in mind their limitations, and especially that in presence of strong, specific solute–solvent interactions, *e.g.* intermolecular hydrogen bonding, they may fail, even dramatically. The illustrative examples that we have discussed in the previous section have been selected to exacerbate these issues. The same examples should have highlighted that both continuum and atomistic approaches are nowadays mature enough to be included within the set of tools exploited in daily chemical research. However, some aspects related to their formulations have not received the attention that should deserve. In fact, almost all formulations of QM/classical methods limit the interaction between the two layers to purely classical terms, *i.e.* electrostatics and polarization. However, as we have showcased for electronic spectroscopies, non-electrostatics may play a relevant role, which might be even more substantial for non-aqueous, low-polarity environments. While a few methods to account for non-electrostatic interactions in QM/continuum or QM/MM energy calculations have been proposed, their inclusion in computed molecular spectra has only been marginally addressed. Remarkably, Pauli repulsion and dispersion effects might be even dominant for magnetic and mixed electric/magnetic (and nuclear) spectra, however to the best of our knowledge, such field is still unexplored.

Conflicts of interest

There are no conflicts to declare.

Notes and references

1 T. Giovannini, F. Egidi and C. Cappelli, *Chem. Soc. Rev.*, 2020, **49**, 5664–5677.
2 M. Bondanza, M. Nottoli, L. Cupellini, F. Lipparini and B. Mennucci, *Phys. Chem. Chem. Phys.*, 2020, **22**, 14433–14448.
3 M. Gaus, Q. Cui and M. Elstner, *J. Chem. Theory Comput.*, 2011, **7**, 931–948.
4 C. Bannwarth, S. Ehlert and S. Grimme, *J. Chem. Theory Comput.*, 2019, **15**, 1652–1671.
5 A. V. Titov, I. S. Ufimtsev, N. Luehr and T. J. Martinez, *J. Chem. Theory Comput.*, 2013, **9**, 213–221.

6 V. Barone, *Computational strategies for spectroscopy: from small molecules to nano systems*, John Wiley & Sons, 2011.

7 F. Egidi, T. Giovannini, G. Del Frate, P. M. Lemler, P. H. Vaccaro and C. Cappelli, *Phys. Chem. Chem. Phys.*, 2019, **21**, 3644–3655.

8 S. Gómez, F. Egidi, A. Puglisi, T. Giovannini, B. Rossi and C. Cappelli, *J. Mol. Liq.*, 2022, **346**, 117841.

9 G. Batignani, E. Mai, G. Fumero, S. Mukamel and T. Scopigno, *Nat. Commun.*, 2022, **13**, 7770.

10 D. A. Fedotov, A. C. Paul, P. Posocco, F. Santoro, M. Garavelli, H. Koch, S. Coriani and R. Improta, *J. Chem. Theory Comput.*, 2021, **17**, 1638–1652.

11 L. Halbert, M. L. Vidal, A. Shee, S. Coriani and A. Severo Pereira Gomes, *J. Chem. Theory Comput.*, 2021, **17**, 3583–3598.

12 A. C. Paul, R. H. Myhre and H. Koch, *J. Chem. Theory Comput.*, 2020, **17**, 117–126.

13 J. Tomasi, B. Mennucci and R. Cammi, *Chem. Rev.*, 2005, **105**, 2999–3094.

14 F. Egidi, V. Barone, J. Bloino and C. Cappelli, *J. Chem. Theory Comput.*, 2012, **8**, 585–597.

15 F. Lipparini, F. Egidi, C. Cappelli and V. Barone, *J. Chem. Theory Comput.*, 2013, **9**, 1880–1884.

16 L. Goletto, S. Gómez, J. H. Andersen, H. Koch and T. Giovannini, *Phys. Chem. Chem. Phys.*, 2022, **24**, 27866–27878.

17 R. Cammi, *Molecular Response Functions for the Polarizable Continuum Model: Physical basis and quantum mechanical formalism*, Springer Science & Business Media, 2013.

18 J. Tomasi, R. Cammi, B. Mennucci, C. Cappelli and S. Corni, *Phys. Chem. Chem. Phys.*, 2002, **4**, 5697–5712.

19 C. Cappelli, *Int. J. Quantum Chem.*, 2016, **116**, 1532–1542.

20 S. Gomez, T. Giovannini and C. Cappelli, *ACS Phys. Chem. Au*, 2023, **3**, 1–16.

21 A. M. Kelley, *Condensed-phase molecular spectroscopy and photophysics*, John Wiley & Sons, 2022.

22 C. Reichardt and T. Welton, *Solvents and solvent effects in organic chemistry*, John Wiley & Sons, 2011.

23 A. Warshel and M. Levitt, *J. Mol. Biol.*, 1976, **103**, 227–249.

24 A. Klamt, *WIREs Comput. Mol. Sci.*, 2011, **1**, 699–709.

25 C. J. Cramer and D. G. Truhlar, *Acc. Chem. Res.*, 2008, **41**, 760–768.

26 T. Giovannini, F. Egidi and C. Cappelli, *Phys. Chem. Chem. Phys.*, 2020, **22**, 22864–22879.

27 P. Lafiosca, S. Gómez, T. Giovannini and C. Cappelli, *J. Chem. Theory Comput.*, 2022, **18**, 1765–1779.

28 S. Ehlert, M. Stahn, S. Spicher and S. Grimme, *J. Chem. Theory Comput.*, 2021, **17**, 4250–4261.

29 S. Ren, F. Lipparini, B. Mennucci and M. Caricato, *J. Chem. Theory Comput.*, 2019, **15**, 4485–4496.

30 M. Caricato, F. Lipparini, G. Scalmani, C. Cappelli and V. Barone, *J. Chem. Theory Comput.*, 2013, **9**, 3035–3042.

31 M. Caricato, *Int. J. Quantum Chem.*, 2019, **119**, e25710.

32 S. Karbalaei Khani, A. Marefat Khah and C. Hattig, *J. Chem. Theory Comput.*, 2020, **16**, 4554–4564.

33 B. Mennucci and S. Corni, *Nat. Rev. Chem.*, 2019, **3**, 315–330.

34 M. Ambrosetti, S. Skoko, T. Giovannini and C. Cappelli, *J. Chem. Theory Comput.*, 2021, **17**, 7146–7156.

35 H. M. Senn and W. Thiel, *Angew. Chem., Int. Ed.*, 2009, **48**, 1198–1229.

36 J. M. H. Olsen and J. Kongsted, *Adv. Quantum Chem.*, 2011, **61**, 107–143.

37 E. R. Kjellgren, J. M. Haugaard Olsen and J. Kongsted, *J. Chem. Theory Comput.*, 2018, **14**, 4309–4319.

38 L. Onsager, *J. Am. Chem. Soc.*, 1936, **58**, 1486–1493.

39 L. Jensen, P. T. van Duijnen and J. G. Snijders, *J. Chem. Phys.*, 2003, **119**, 12998–13006.

40 J. Nicoli, T. Giovannini and C. Cappelli, *J. Chem. Phys.*, 2022, **157**, 214101.

41 J. M. Herbert, *WIREs Comput. Mol. Sci.*, 2021, **11**, e1519.

42 O. Andreussi and G. Fisicaro, *Int. J. Quantum Chem.*, 2019, **119**, e25725.

43 C. Amovilli, V. Barone, R. Cammi, E. Cancès, M. Cossi, B. Mennucci, C. S. Pomelli and J. Tomasi, *Adv. Quantum Chem.*, 1998, **32**, 227–261.

44 C. S. Pomelli, *Continuum Solvation Models in Chemical Physics: From Theory to Applications*, 2008, 49.

45 R. Cammi and J. Tomasi, *J. Comput. Chem.*, 1995, **16**, 1449–1458.

46 E. Cances, B. Mennucci and J. Tomasi, *J. Chem. Phys.*, 1997, **107**, 3032–3041.

47 R. Di Remigio, M. T. Beerepoot, Y. Cornaton, M. Ringholm, A. H. Steindal, K. Ruud and L. Frediani, *Phys. Chem. Chem. Phys.*, 2017, **19**, 366–379.

48 C. Amovilli and B. Mennucci, *J. Phys. Chem. B*, 1997, **101**, 1051–1057.

49 F. Floris, J. Tomasi and J. P. Ahuir, *J. Comput. Chem.*, 1991, **12**, 784–791.

50 C. Hille, S. Ringe, M. Deimel, C. Kunkel, W. E. Acree, K. Reuter and H. Oberhofer, *J. Chem. Phys.*, 2019, **150**, 041710.

51 A. Pomogaeva and D. M. Chipman, *J. Phys. Chem. A*, 2013, **117**, 5812–5820.

52 A. Pomogaeva and D. M. Chipman, *J. Chem. Theory Comput.*, 2014, **10**, 211–219.

53 Z.-Q. You and J. M. Herbert, *J. Chem. Theory Comput.*, 2016, **12**, 4338–4346.

54 A. S. Perera, J. Thomas, M. R. Poopari and Y. Xu, *Front. Chem.*, 2016, **4**, 9.

55 T. Vreven, B. Mennucci, C. da Silva, K. Morokuma and J. Tomasi, *J. Chem. Phys.*, 2001, **115**, 62–72.

56 C. Curutchet, A. Muñoz-Losa, S. Monti, J. Kongsted, G. D. Scholes and B. Mennucci, *J. Chem. Theory Comput.*, 2009, **5**, 1838–1848.

57 J. M. Olsen, K. Aidas and J. Kongsted, *J. Chem. Theory Comput.*, 2010, **6**, 3721–3734.

58 J. M. H. Olsen, C. Steinmann, K. Ruud and J. Kongsted, *J. Phys. Chem. A*, 2015, **119**, 5344–5355.

59 A. H. Steindal, K. Ruud, L. Frediani, K. Aidas and J. Kongsted, *J. Phys. Chem. B*, 2011, **115**, 3027–3037.

60 P. Reinholdt, J. Kongsted and J. M. H. Olsen, *J. Phys. Chem. Lett.*, 2017, **8**, 5949–5958.

61 T. Schwabe, J. M. H. Olsen, K. Sneskov, J. Kongsted and O. Christiansen, *J. Chem. Theory Comput.*, 2011, **7**, 2209–2217.

62 D. Loco, É. Polack, S. Caprasecca, L. Lagardere, F. Lipparini, J.-P. Piquemal and B. Mennucci, *J. Chem. Theory Comput.*, 2016, **12**, 3654–3661.

63 L. Jensen, P. T. Van Duijnen and J. G. Snijders, *J. Chem. Phys.*, 2003, **119**, 3800–3809.

64 L. Jensen, P. T. Van Duijnen and J. G. Snijders, *J. Chem. Phys.*, 2003, **118**, 514–521.

65 R. A. Bryce, R. Buesnel, I. H. Hillier and N. A. Burton, *Chem. Phys. Lett.*, 1997, **279**, 367–371.

66 R. Sanderson, *Science*, 1951, **114**, 670–672.

67 P. Geerlings, S. Fias, Z. Boisdenghien and F. De Proft, *Chem. Soc. Rev.*, 2014, **43**, 4989–5008.

68 T. Giovannini, A. Puglisi, M. Ambrosetti and C. Cappelli, *J. Chem. Theory Comput.*, 2019, **15**, 2233–2245.

69 T. Giovannini, L. Grazioli, M. Ambrosetti and C. Cappelli, *J. Chem. Theory Comput.*, 2019, **15**, 5495–5507.

70 F. Lipparini, C. Cappelli, G. Scalmani, N. De Mitri and V. Barone, *J. Chem. Theory Comput.*, 2012, **8**, 4270–4278.

71 F. Lipparini, C. Cappelli and V. Barone, *J. Chem. Theory Comput.*, 2012, **8**, 4153–4165.

72 F. Lipparini, C. Cappelli and V. Barone, *J. Chem. Phys.*, 2013, **138**, 234108.

73 T. Giovannini, M. Olszòwka, F. Egidi, J. R. Cheeseman, G. Scalmani and C. Cappelli, *J. Chem. Theory Comput.*, 2017, **13**, 4421–4435.

74 T. Giovannini, G. Del Frate, P. Lafiosca and C. Cappelli, *Phys. Chem. Chem. Phys.*, 2018, **20**, 9181–9197.

75 A. Stone, *The theory of intermolecular forces*, OUP Oxford, 2013.

76 R. McWeeny, *Methods of molecular quantum mechanics*, Academic press, London, 1992.

77 M. S. Gordon, L. Slipchenko, H. Li and J. H. Jensen, *Annu. Rep. Comput. Chem.*, 2007, **3**, 177–193.

78 A. DeFusco, N. Minezawa, L. V. Slipchenko, F. Zahariev and M. S. Gordon, *J. Phys. Chem. Lett.*, 2011, **2**, 2184–2192.

79 D. Kosenkov and L. V. Slipchenko, *J. Phys. Chem. A*, 2011, **115**, 392–401.

80 T. Giovannini, P. Lafiosca and C. Cappelli, *J. Chem. Theory Comput.*, 2017, **13**, 4854–4870.

81 C. Amovilli and F. M. Floris, *Phys. Chem. Liq.*, 2020, **58**, 281–289.

82 F. M. Floris and C. Amovilli, *Mol. Phys.*, 2020, **118**, e1752401.

83 T. Giovannini, P. Lafiosca, B. Chandramouli, V. Barone and C. Cappelli, *J. Chem. Phys.*, 2019, **150**, 124102.

84 T. Giovannini, M. Ambrosetti and C. Cappelli, *J. Phys. Chem. Lett.*, 2019, **10**, 5823–5829.

85 G. Marrazzini, T. Giovannini, F. Egidi and C. Cappelli, *J. Chem. Theory Comput.*, 2020, **16**, 6993–7004.

86 C. Amovilli and F. M. Floris, *J. Chem. Theory Comput.*, 2022, **18**, 6816–6825.

87 L. Cupellini, C. Amovilli and B. Mennucci, *J. Phys. Chem. B*, 2014, **119**, 8984–8991.

88 K. Burke, *J. Chem. Phys.*, 2012, **136**, 150901.

89 A. Laio and M. Parrinello, *Proc. Natl. Acad. Sci. U. S. A.*, 2002, **99**, 12562–12566.

90 R. Cammi, B. Mennucci and J. Tomasi, *J. Phys. Chem. A*, 1998, **102**, 870–875.

91 B. Mennucci, C. Cappelli, R. Cammi and J. Tomasi, *Chirality*, 2011, **23**, 717–729.

92 F. Egidi, T. Giovannini, M. Piccardo, J. Bloino, C. Cappelli and V. Barone, *J. Chem. Theory Comput.*, 2014, **10**, 2456–2464.

93 N. H. List, H. J. A. Jensen and J. Kongsted, *Phys. Chem. Chem. Phys.*, 2016, **18**, 10070–10080.

94 N. H. List, J. M. H. Olsen and J. Kongsted, *Phys. Chem. Chem. Phys.*, 2016, **18**, 20234–20250.

95 Z.-Q. You, J.-M. Mewes, A. Dreuw and J. M. Herbert, *J. Chem. Phys.*, 2015, **143**, 204104.

96 S. K. Paul, M. P. Coons and J. M. Herbert, *J. Chem. Phys.*, 2019, **151**, 189901.

97 S. K. Paul and J. M. Herbert, *J. Am. Chem. Soc.*, 2021, **143**, 10189–10202.

98 T. Giovannini, R. R. Riso, M. Ambrosetti, A. Puglisi and C. Cappelli, *J. Chem. Phys.*, 2019, **151**, 174104.

99 T. Giovannini, M. Macchiagodena, M. Ambrosetti, A. Puglisi, P. Lafiosca, G. Lo Gerfo, F. Egidi and C. Cappelli, *Int. J. Quantum Chem.*, 2019, **119**, e25684.

100 Z. Rinkevicius, X. Li, J. A. Sandberg, K. V. Mikkelsen and H. Ågren, *J. Chem. Theory Comput.*, 2014, **10**, 989–1003.

101 T. Schwabe, *J. Chem. Phys.*, 2016, **145**, 154105.

102 H. Schroder and T. Schwabe, *J. Chem. Theory Comput.*, 2018, **14**, 833–842.

103 M. Caricato, B. Mennucci, J. Tomasi, F. Ingrosso, R. Cammi, S. Corni and G. Scalmani, *J. Chem. Phys.*, 2006, **124**, 124520.

104 A. V. Marenich, C. J. Cramer, D. G. Truhlar, C. A. Guido, B. Mennucci, G. Scalmani and M. J. Frisch, *Chem. Sci.*, 2011, **2**, 2143–2161.

105 J.-M. Mewes, Z.-Q. You, M. Wormit, T. Kriesche, J. M. Herbert and A. Dreuw, *J. Phys. Chem. A*, 2015, **119**, 5446–5464.

106 J.-M. Mewes, J. M. Herbert and A. Dreuw, *Phys. Chem. Chem. Phys.*, 2017, **19**, 1644–1654.

107 C. A. Guido, A. Chrayteh, G. Scalmani, B. Mennucci and D. Jacquemin, *J. Chem. Theory Comput.*, 2021, **17**, 5155–5164.

108 S. Skoko, C. Micheletti, E. Grifoni, F. Egidi, T. Giovannini, A. Pucci and C. Cappelli, *Dyes Pigm.*, 2023, DOI: 10.1016/j.dyepig.2023.111227.

109 V. Barone, J. Bloino, S. Monti, A. Pedone and G. Prampolini, *Phys. Chem. Chem. Phys.*, 2011, **13**, 2160–2166.

110 M. Cossi and V. Barone, *J. Chem. Phys.*, 1998, **109**, 6246–6254.

111 R. Cammi, C. Cappelli, S. Corni and J. Tomasi, *J. Phys. Chem. A*, 2000, **104**, 9874–9879.

112 S. Corni, C. Cappelli, R. Cammi and J. Tomasi, *J. Phys. Chem. A*, 2001, **105**, 8310–8316.

113 C. Cappelli, S. Corni, R. Cammi, B. Mennucci and J. Tomasi, *J. Chem. Phys.*, 2000, **113**, 11270–11279.

114 C. Cappelli, S. Corni and J. Tomasi, *J. Chem. Phys.*, 2001, **115**, 5531–5535.

115 K. O. H. M. Dundas, M. T. Beerepoot, M. Ringholm, S. Reine, R. Bast, N. H. List, J. Kongsted, K. Ruud and J. M. H. Olsen, *J. Chem. Theory Comput.*, 2021, **17**, 3599–3617.

116 T. Giovannini, M. Olszowka and C. Cappelli, *J. Chem. Theory Comput.*, 2016, **12**, 5483–5492.

117 N. A. Besley and J. A. Bryan, *J. Phys. Chem. C*, 2008, **112**, 4308–4314.

118 A. Segalina, J. Cerezo, G. Prampolini, F. Santoro and M. Pastore, *J. Chem. Theory Comput.*, 2020, **16**, 7061–7077.

119 Q. Xu, D. Aranda, M. Yaghoubi Jouybari, Y. Liu, M. Wang, J. Cerezo, R. Improta and F. Santoro, *J. Phys. Chem. A*, 2022, **126**, 7468–7479.

120 W. Chen, P. Zhang, D. G. Truhlar, J. Zheng and X. Xu, *J. Chem. Theory Comput.*, 2022, **18**, 7671–7682.

121 I. Carnimeo, C. Puzzarini, N. Tasinato, P. Stoppa, A. P. Charmet, M. Biczysko, C. Cappelli and V. Barone, *J. Chem. Phys.*, 2013, **139**, 074310.

122 C. Cappelli, F. Lipparini, J. Bloino and V. Barone, *J. Chem. Phys.*, 2011, **135**, 104505.

123 R. Cammi, B. Mennucci and J. Tomasi, *J. Chem. Phys.*, 1999, **110**, 7627–7638.

124 H. Solheim, L. Frediani, K. Ruud and S. Coriani, *Theor. Chem. Acc.*, 2008, **119**, 231–244.

125 P. Reinholdt, M. S. Nørby and J. Kongsted, *J. Chem. Theory Comput.*, 2018, **14**, 6391–6404.

126 P. Norman, K. Ruud and T. Saue, *Principles and practices of molecular properties: Theory, modeling, and simulations*, John Wiley & Sons, 2018.

127 T. Helgaker, M. Jaszunski and K. Ruud, *Chem. Rev.*, 1999, **99**, 293–352.

128 R. Cammi, *J. Chem. Phys.*, 1998, **109**, 3185–3196.

129 P. Carey, *Biochemical applications of Raman and resonance Raman spectroscopes*, Elsevier, 2012.

130 F. Santoro, C. Cappelli and V. Barone, *J. Chem. Theory Comput.*, 2011, **7**, 1824–1839.

131 F. F. Avila, V. Barone, C. Cappelli and F. Santoro, *J. Chem. Theory Comput.*, 2013, **9**, 3597–3611.

132 F. Egidi, J. Bloino, C. Cappelli and V. Barone, *J. Chem. Theory Comput.*, 2014, **10**, 346–363.

133 B. Mennucci, C. Cappelli, R. Cammi and J. Tomasi, *Theor. Chem. Acc.*, 2007, **117**, 1029–1039.

134 S. Gómez, C. Bottari, F. Egidi, T. Giovannini, B. Rossi and C. Cappelli, *J. Phys. Chem. Lett.*, 2022, **13**, 6200–6207.

135 S. Gómez, N. Rojas-Valencia, T. Giovannini, A. Restrepo and C. Cappelli, *Molecules*, 2022, **27**, 442.

136 A. M. Kelley, *J. Phys. Chem. A*, 1999, **103**, 6891–6903.

137 F. Egidi, J. Bloino, C. Cappelli and V. Barone, *J. Chem. Theory Comput.*, 2013, **10**, 346–363.

138 P. L. Polavarapu, *Chiroptical spectroscopy: fundamentals and applications*, Crc Press, 2016.

139 L. A. Nafie, *Vibrational optical activity: principles and applications*, John Wiley & Sons, Chichester, 2011.

140 P. J. Stephens, F. J. Devlin and J. R. Cheeseman, *VCD spectroscopy for organic chemists*, CRC Press, 2012.

141 P. L. Polavarapu, *Chem. Rec.*, 2007, **7**, 125–136.

142 M. Krupová, J. Kessler and P. Bouř, *ChemPlusChem*, 2020, **85**, 561–575.

143 C. Cappelli, J. Bloino, F. Lipparini and V. Barone, *J. Phys. Chem. Lett.*, 2012, **3**, 1766–1773.

144 C. Cappelli, S. Corni, B. Mennucci, R. Cammi and J. Tomasi, *J. Phys. Chem. A*, 2002, **106**, 12331–12339.

145 M. Pecul, E. Lamparska, C. Cappelli, L. Frediani and K. Ruud, *J. Phys. Chem. A*, 2006, **110**, 2807–2815.

146 S. Pipolo, R. Cammi, A. Rizzo, C. Cappelli, B. Mennucci and J. Tomasi, *Int. J. Quantum Chem.*, 2011, **111**, 826–838.

147 F. Egidi, R. Russo, I. Carnimeo, A. D'Urso, G. Mancini and C. Cappelli, *J. Phys. Chem. A*, 2015, **119**, 5396–5404.

148 S. Jurinovich, G. Pescitelli, L. Di Bari and B. Mennucci, *Phys. Chem. Chem. Phys.*, 2014, **16**, 16407–16418.

149 R. Di Remigio, A. H. Steindal, K. Mozgawa, V. Weijo, H. Cao and L. Frediani, *Int. J. Quantum Chem.*, 2019, **119**, e25685.

150 M. Scheurer, P. Reinholdt, E. R. Kjellgren, J. M. Haugaard Olsen, A. Dreuw and J. Kongsted, *J. Chem. Theory Comput.*, 2019, **15**, 6154–6163.

151 *ADF 2021.1, SCM, Theoretical Chemistry*, Vrije Universiteit, Amsterdam, The Netherlands, http://www.scm.com.

152 G. te Velde, F. M. Bickelhaupt, E. J. Baerends, C. Fonseca Guerra, S. J. A. van Gisbergen, J. G. Snijders and T. Ziegler, *J. Comput. Chem.*, 2001, **22**, 931–967.

153 *AMS 2021.1, SCM, Theoretical Chemistry*, Vrije Universiteit, Amsterdam, The Netherlands, http://www.scm.com.

154 QM/FQ coupled to MD sampling, last access 29/12/2022, https://www.scm.com/doc/Tutorials/OpticalPropertiesElectronicExcitations/QMFQ_MD.html.

155 C. Reichardt, *Chem. Rev.*, 1994, **94**, 2319–2358.

156 J. O. Morley, R. M. Morley and A. L. Fitton, *J. Am. Chem. Soc.*, 1998, **120**, 11479–11488.

157 V. Cavalli, D. C. da Silva, C. Machado, V. G. Machado and V. Soldi, *J. Fluoresc.*, 2006, **16**, 77–86.

158 A. V. Marenich, C. J. Cramer and D. G. Truhlar, *J. Phys. Chem. B*, 2015, **119**, 958–967.

159 M. Biczysko, J. Bloino, G. Brancato, I. Cacelli, C. Cappelli, A. Ferretti, A. Lami, S. Monti, A. Pedone, G. Prampolini, C. Puzzarini, F. Santoro, F. Trani and G. Villani, *Theor. Chem. Acc.*, 2012, **131**, 1201.

160 Z.-L. Cai and J. R. Reimers, *J. Phys. Chem. A*, 2000, **104**, 8389–8408.

161 K. J. de Almeida, K. Coutinho, W. B. De Almeida, W. R. Rocha and S. Canuto, *Phys. Chem. Chem. Phys.*, 2001, **3**, 1583–1587.

162 C. Cappelli, B. Mennucci and S. Monti, *J. Phys. Chem. A*, 2005, **109**, 1933–1943.

163 A. Edelmann and B. Lendl, *J. Am. Chem. Soc.*, 2002, **124**, 14741–14747.

164 M. Losada and Y. Xu, *Phys. Chem. Chem. Phys.*, 2007, **9**, 3127–3135.

165 G. Cassanas, M. Morssli, E. Fabregue and L. Bardet, *J. Raman Spectrosc.*, 1991, **22**, 409–413.

166 B. Mennucci, *J. Am. Chem. Soc.*, 2002, **124**, 1506–1515.

167 M. Witanowski, W. Sicinska, S. Biernat and G. Webb, *J. Magn. Res.*, 1991, **91**, 289–300.

168 X. G. Chen, S. A. Asher, R. Schweitzer-Stenner, N. G. Mirkin and S. Krimm, *J. Am. Chem. Soc.*, 1995, **117**, 2884–2895.

169 L. C. Mayne and B. Hudson, *J. Phys. Chem.*, 1991, **95**, 2962–2967.

170 N. E. Triggs and J. J. Valentini, *J. Phys. Chem.*, 1992, **96**, 6922–6931.

171 N. S. Myshakina, Z. Ahmed and S. A. Asher, *J. Phys. Chem. B*, 2008, **112**, 11873–11877.

172 P. Mukhopadhyay, G. Zuber, P. Wipf and D. N. Beratan, *Angew. Chem., Int. Ed.*, 2007, **46**, 6450–6452.

173 Y. Kumata, J. Furukawa and T. Fueno, *Bull. Chem. Soc. Jpn.*, 1970, **43**, 3920–3921.

174 R. D'Cunha and T. D. Crawford, *J. Phys. Chem. A*, 2021, **125**, 3095–3108.

175 P. Mukhopadhyay, G. Zuber, M.-R. Goldsmith, P. Wipf and D. N. Beratan, *Chem. Phys. Chem.*, 2006, **7**, 2483–2486.

176 M. Diem, *J. Am. Chem. Soc.*, 1988, **110**, 6967–6970.